

ORIGINAL ARTICLE

Open Access



Efficient Preparation of Nanoparticle-Reinforced Nickel-based Composite Coating with Highly Preferred (220) Orientation

Renjie Ji¹ , Hui Jin¹, Yonghong Liu^{1,2*}, Tiancong Dong¹, Fan Zhang¹, Lilong Zhao¹, Xinlei Wu¹, Qiang Sun¹, Peng Liu¹, Hang Dong¹, Chi Ma¹, Dege Li¹ and Baoping Cai¹

Abstract

Nanoparticle-reinforced metal matrix composite coatings have significant potential in mechanical part surface strengthening owing their excellent mechanical properties. This paper reports a phenomenon in which the grain orientation gradually evolves to (220) as the deposition current density increases when preparing nanoparticle-reinforced nickel-based composite coatings through jet electrodeposition (JED). During the preparation of the Ni-SiC composite coatings, the deposition current density increased from 180 A/dm² to 220 A/dm², and TC(220) gradually increase from 41.4% to 97.7%. With an increase of TC(220), the self-corrosion potential increases from -0.575 to -0.477 V, the corrosion current density decreases from 9.52 μA/cm² to 2.76 μA/cm², the diameter of the corrosion pits that after 10 days of immersion in a 3.5 wt% NaCl solution decreases from 278–944 nm to 153–260 nm, and the adhesion of the coating increases from 24.9 N to 61.6 N. Compared a conventional electrodeposition (CED), the Ni-SiC composite coating using JED has the advantages of a smooth surface morphology, high corrosion resistance, and strong adhesion, which are more obvious with an increase in TC(220).

Keywords: Jet electrodeposition, Composite coating, Preferred orientation, Adhesion force, Corrosion resistance

1 Introduction

With the continuous development of modern industry, the wear and corrosion resistances of an increasing number of key components of high-end equipment are required; thus, high-performance composite coatings usually need to be prepared on the key component surface. Nanoparticle-reinforced metal matrix composite coatings have significant potential application in surface strengthening of mechanical parts owing to their excellent hardness, abrasion resistance, corrosion resistance,

and high-temperature oxidation resistance. Researchers are widely concerned with this issue. Li et al. [1] produced a Ni-SiO₂ composite coating by electrodeposition and found that the addition of SiO₂ nanoparticles improves the wear resistance of the coating. Li et al. [2] prepared a Ni-W/TiN coating by pulse electrodeposition and observed that the doped TiN nanoparticles promote nucleation and cause obvious changes in the microstructure, thus improving the hardness and corrosion resistance of the coating. Tao et al. [3] fabricated a Ni-B-Sc coating using conventional electrodeposition and detected that the grain boundary and phase boundary area increased owing to the addition of Ni₂Sc nanoparticles. However, nanoparticles usually exist in the form of agglomeration in the plating solution because of their high surface energy. It is difficult to break the

*Correspondence: liuyhpc@163.com

[†]Renjie Ji and Hui Jin contributed equally to this work and should be considered as co-first authors

¹ College of Mechanical and Electronic Engineering, China University of Petroleum (East China), Qingdao 266580, China

Full list of author information is available at the end of the article

agglomeration of nanoparticles by conventional electro-deposition, and thus the prepared composite coatings have defects, such as rough surfaces and poor adhesion [4, 5].

JED is a type of unconventional electrodeposition. The high-speed jet liquid improves the transmission speed of ions in the deposition process compared with CED. The ions are evenly distributed by high-speed flushing, which reduces the concentration polarization and improves the upper limit value of the current density during the electrodeposition process [6, 7]. Meanwhile, the agglomeration of the nanoparticles is broken up during high-speed flushing, and the nanoparticles are distributed uniformly in the coating. Therefore, using JED to prepare nanoparticle-reinforced composite coating, the advantages of a high deposition efficiency, uniform nanoparticles distribution, and good quality of the coating can be obtained [8–10].

During electrodeposition, the preferred orientation (texture) often occurs, which means that significant amounts of grains exhibit the same common orientation characteristics in the deposition layer. This is called a highly preferred orientation if almost all of the grains are assembled in one certain orientation. By controlling the preferred orientation of the grains in the deposition layer, the properties of the deposition layer can be improved, and even the deposition layer has some special functions. Gao et al. [11] fabricated Co-Ni films with a preferred (220) orientation by controlling the variation of the Co and Ni ratio, which showed a superior photocatalytic performance. Ponrouch et al. [12] prepared preferentially oriented (100) platinum nanowires and thin films by changing the deposition potential, which exhibited efficient electrocatalytic properties. Kim et al. [13] manufactured $\text{Bi}_2\text{Te}_{3-x}\text{Se}_x$ thin films using pulse electrodeposition. By changing the duty cycle of the current, thin films achieved a preferred orientation of (110), and displayed a superior thermoelectric performance.

In recent years, research on the preferred orientation of nickel coatings using CED has attracted significant attention. Calderón et al. [14] carried out an experiment on the preparation of Ni-SiC composite coatings. It was found that with an increase in the SiC content, the grain orientation of the coatings gradually evolved from (200) to (111), and the corrosion resistance of the coating improved with the grain orientation of (111). Zhao et al. [15] studied Ni-xAl-yTi composite coatings, and claimed that as the content of Al and Ti particles increased, the orientation of (200) decreased while (111) increased; in addition, the preferred (111) orientation coating showed a better corrosion resistance than the preferred (200) orientation. Alizadeh et al. [16] conducted an analysis on Ni-Cu/ Al_2O_3 composite coatings. They reported

that the structure of the coatings gradually evolved to a preferred (111) orientation when the Al_2O_3 content increased, and the hardness, wear resistance, and corrosion resistance of the coatings were improved. Deng et al. [17] demonstrated that with the addition of 1,4-bis(2-hydroxyethoxy)-2-butyne (BEO), the grains preferred the orientation of Ni/diamond composite coatings over a (200) orientation, and the wear resistance of the coating was also enhanced.

The above studies on the preferred orientation of nickel-based composite coatings mainly focused on (111) and (200) orientations, and little research has been conducted on the highly preferred (220) orientation. This paper reveals the efficient preparation of nanoparticle-reinforced nickel-based composite coating with a highly preferred (220) orientation, and then explores the effect of the deposition parameters on the structure of nanoparticle-reinforced nickel-based composite coatings. Because of the high hardness and stability of SiC nanoparticles, Ni-SiC composite coatings have been widely used [18]. This paper focused on the properties of Ni-SiC composite coatings. The microstructure, corrosion resistance, and the adhesion force of the Ni-SiC composite coating with a highly preferred (220) orientation were investigated. Some innovative theoretical and technological achievements were made.

2 Experiment

2.1 Principle of Efficient Preparation of Nanoparticles

Reinforced Nickel-Based Composite Coating by JED

The experimental device for JED is shown in Figure 1a. The pure titanium rod connects to the positive pole of the DC power supply, and the substrate connects to the negative pole of the DC power supply. The pure titanium rod acts as the current transfer electrode, which transfers the current to nickel balls, making the nickel balls become an anode. Nickel atoms are oxidized into a large amount of Ni^{2+} , which is used to supplement the Ni^{2+} that is constantly consumed during the plating solution. The titanium rod is not consumed in experiments because the chemical properties of the titanium rod are more stable than those of the nickel balls. Because the titanium rod is closer to the upper surface of the substrate, the unconsumed titanium rod can help provide a stable electric field environment, and the deposited coatings achieve a better uniformity. The plating solution in the liquid storage tank is heated by a water bath to maintain a constant temperature. During the preparation process, the composite plating solution is first transported to the anode cylinder through the inlet pipe by a diaphragm pump. The plating solution in the anode cylinder is then impacted on the substrate through the nozzle at a high

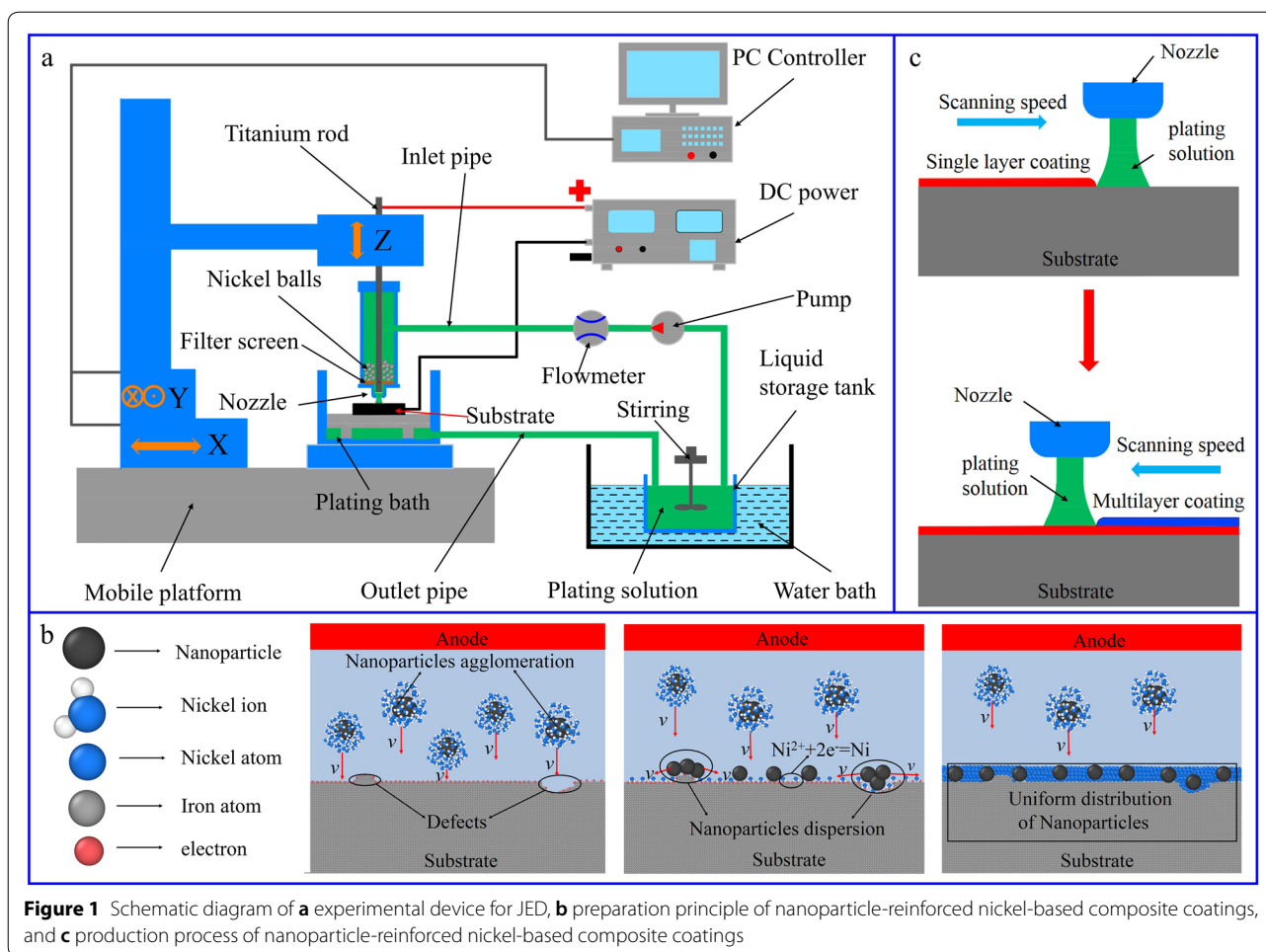


Figure 1 Schematic diagram of **a** experimental device for JED, **b** preparation principle of nanoparticle-reinforced nickel-based composite coatings, and **c** production process of nanoparticle-reinforced nickel-based composite coatings

speed for deposition. Finally, the plating solution flows back to the liquid storage tank through the outlet pipe.

A schematic diagram of the preparation principle of nanoparticle-reinforced nickel-based composite coatings using JED is illustrated in Figure 1b. Most of the nanoparticles exist in the plating solution as an agglomeration, which is mainly surrounded by water molecules and ion clusters. Because the main chemical reaction is the redox of Ni^{2+} during electrodeposition, the model is simplified into a nanoparticle agglomeration surrounded by a large number of Ni^{2+} ions. When the nanoparticle agglomeration is impacted by the substrate at a high speed, the nanoparticle agglomeration is divided into many individual nanoparticles owing to the reacting force. According to the composite co-deposition theory [19, 20], some nanoparticles are adsorbed on the substrate, among which the strongly adsorbed nanoparticles are deposited and the weakly adsorbed nanoparticles are washed away. Meanwhile, under the condition of a high deposition current density, a large amount of Ni^{2+} near the cathode is reduced to Ni atoms, and then Ni atoms

are then deposited on the substrate. The stacking of Ni atoms and nanoparticles covering the substrate rapidly becomes defective, and eventually a nanoparticle-reinforced nickel-based composite coating with a smooth surface is formed.

As shown in Figure 1c, the thickness of the coating increases gradually when the nozzle moves back and forth along the path at a certain scanning speed. The required thickness and shape of the composite coating are obtained by controlling the nozzle path and deposition time.

2.2 Experimental Parameters Applied in the Preparation of Nanoparticle-Reinforced Nickel-Based Composite Coating Using JED

The composition of the plating solution and the experimental parameters are shown in Table 1. The purity of the SiC nanoparticles was 99.99% and the average particle size was approximately 50 nm as shown in Figure 2a and b. SEM figures are also shown in Figure 2a and b. The substrate material was a medium-carbon steel. The

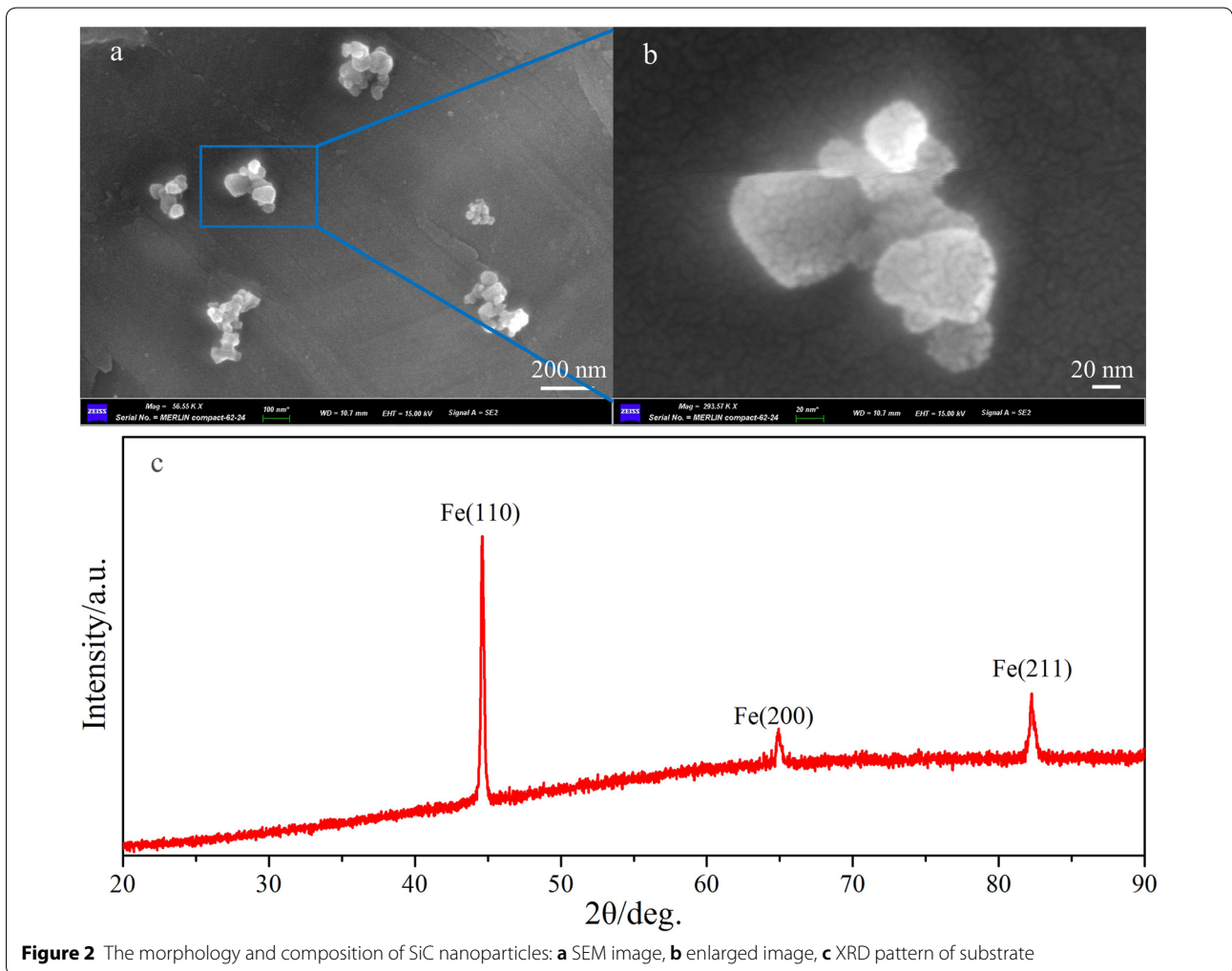
Table 1 Composition of plating solution and experimental parameters

Composition and parameters	Quantity
NiSO ₄ ·6H ₂ O (g/L)	300
NiCl ₂ ·6H ₂ O (g/L)	40
H ₃ BO ₄ (g/L)	40
Saccharin (g/L)	0.5
Emulsifier OP-10 (g/L)	1.0
SiC nano-particles (g/L)	3.0
pH value	4.0
Nozzle diameter (mm)	5.0
Scanning speed of nozzle (mm/min)	100
Distance between nozzle and cathode (mm)	3.0
Injection velocity (m/s)	1.40–2.65
Current density (A/dm ²)	180–220
Temperature (°C)	60

substrate was pretreated before the experiment, the process of which is as follows: fine grinding, - oil removal, - acetone ultrasonic cleaning, - alcohol ultrasonic cleaning, - deionized water ultrasonic cleaning, - and drying. An XRD pattern of the substrate is shown in Figure 2c.

2.3 Test details

The grain orientation and grain size of the nanoparticle-reinforced nickel-based composite coatings were characterized using X-ray diffraction (XRD, X’Pert Pro MPD) with Cu-Kα (λ = 0.154184 nm) radiation, and the test parameters were a voltage of 45 kV, current of 40 mA, scanning range of 20° to 90°, step width of 0.01°, and scanning speed of 10°/min. The adhesion force of the nanoparticle-reinforced nickel-based composite coatings were quantitatively tested using a scratch tester (WS-2004). The test was carried out in the form of dynamic loading. The scratch length was 4 mm, and the diamond tool was uniformly loaded from 0 to 70 N at a loading



rate of 70/4 N/mm. The morphology and elemental content of the nanoparticle-reinforced nickel-based composite coatings were measured using scanning electron microscopy with energy dispersive spectroscopy (SEM, EDS, ZEISS MERLIN Compact). The surface roughness of nanoparticle-reinforced nickel-based composite coatings were measured using TR300 Roughness Measuring Instrument with a sampling length of 4 mm. The electrochemical properties of the Ni-SiC composite coatings were evaluated using electrochemical workstation (CHI 760e) in a 3.5 wt% NaCl solution at room temperature. The test samples were Ni-SiC composite coatings with an area of 1 cm². A saturated calomel electrode, platinum plate and samples were used as the reference electrode, counter electrode and working electrode, respectively. The polarization curves were recorded within the potential range of -150 to +350 mV (compared to the Eocp) at a scan rate of 0.002 V/s and a scan frequency of 2 Hz. Electrochemical impedance spectroscopy (EIS) investigations were conducted at sinusoidal signal amplitude of 10 mV and at a frequency range of 10⁵ to 10⁻² Hz. Full immersion corrosion tests of the Ni-SiC composite coatings are carried out. The corrosion solution was a 3.5 wt% NaCl solution, and the corrosion time were 1, 3, 5, and 10 days.

3 Results and Discussion

3.1 Grain Orientation Evolution of Ni-SiC Composite Coating during JED

During the JED process, the deposition layer is rapidly formed on the surface of the substrate under the condition of high current density by means of high-speed jetting. Therefore, the injection velocity and current density are important parameters influencing the structure of the coatings. In this study, a large number of Ni-SiC composite coatings were one produced at different current densities and injection velocities. The thicknesses of these coatings were controlled to approximately 50 μm by changing the deposition time. According to Figure 3a-e, the XRD patterns of the Ni-SiC composite coatings prepared using JED under different deposition parameters all present clear diffraction peaks of Ni(111), Ni(200), and Ni(220). It can be seen that with an increase in the deposition current density from 180 A/dm² to 220 A/dm², the coating orientation shows a trend of gradual evolution to Ni(220). The XRD pattern of the Ni-SiC composite coating prepared using CED is shown in Figure 3f, which indicates a Ni-SiC composite coating without a highly preferred (220) orientation.

The preferred orientation coefficient (texture coefficients) of different crystal planes in these coatings are calculated using Eq. (1) [21], where TC(hkl) is the texture coefficient of the (hkl) orientation, I(hkl) is the measured

intensity of (hkl) reflection, I₀(hkl) is the powder diffraction intensity of nickel (PDF#70-0989), and n is the number of reflections used in the calculations. In this case, (111), (200) and (220) peaks were used for the texture coefficient calculation (n = 3).

$$TC(hkl) = \frac{I_{(hkl)}/I_{0(hkl)}}{\sum_{i=1}^n I_{(hkl)}/I_{0(hkl)}} \quad (1)$$

The grain sizes of these coatings are calculated using Eq. (2) [22], where D(hkl) represents the grain size of the (hkl) orientation, B represents the half-height width of diffraction peak (degree), γ represents the wavelength of Cu-Kα (λ = 0.154184 nm), θ is the Bragg angle (rad) and K is a constant (K = 0.89).

$$D(hkl) = \frac{K\gamma}{B \cos \theta} \quad (2)$$

Figure 4a-c shows the variations in TC (111), TC (200), and TC(220) of Ni-SiC composite coatings prepared using JED under different deposition parameters. When the current density increases, it shows a general trend in which TC(111) and TC(200) gradually decreases and TC (220) gradually increases. Under low current density conditions (180–200 A/dm²), the TC (111), TC (200) and TC(220) are significantly affected by variations in the injection velocity. As the injection velocity increased, TC (111) and TC(200) first decreased and then increased, and TC(220) first increased and then decreased. However, at a higher deposition current density (>200 A/dm²), the grain orientation of the coatings is slightly affected by the variation of the injection velocity, and TC (111), TC (200) and TC (220) remain stable. Under the deposition conditions of 220 A/dm² current density and 1.76 m/s injection velocity, TC (220) reached a maximum of 97.7%.

As shown in Figure 4d, it can be seen that the variation range of D(111) and D(200) is small as the current density increases. The value of D(111) is between 19 and 20 nm and D(200) is between 17 and 18 nm. Unlike D(111) and D(200), D(220) increases with an increase in the deposition current density. When the deposition current density is 180 A/dm², the average value of D(220) is 47.5 nm. As the deposition current density increase to 220 A/dm², the average value of D(220) increase to 61.6 nm.

As shown in Figure 5, during the preparation of nanoparticle-reinforced nickel-based composite coatings using JED, Ni atoms are stacked with face-centered cubic structure cells. Usually, these cells are deposited on the substrate surface with the (111), (200), and (220) crystal-line planes. The selection of the grain orientation mainly depends on the cathodic overpotential, which is mainly

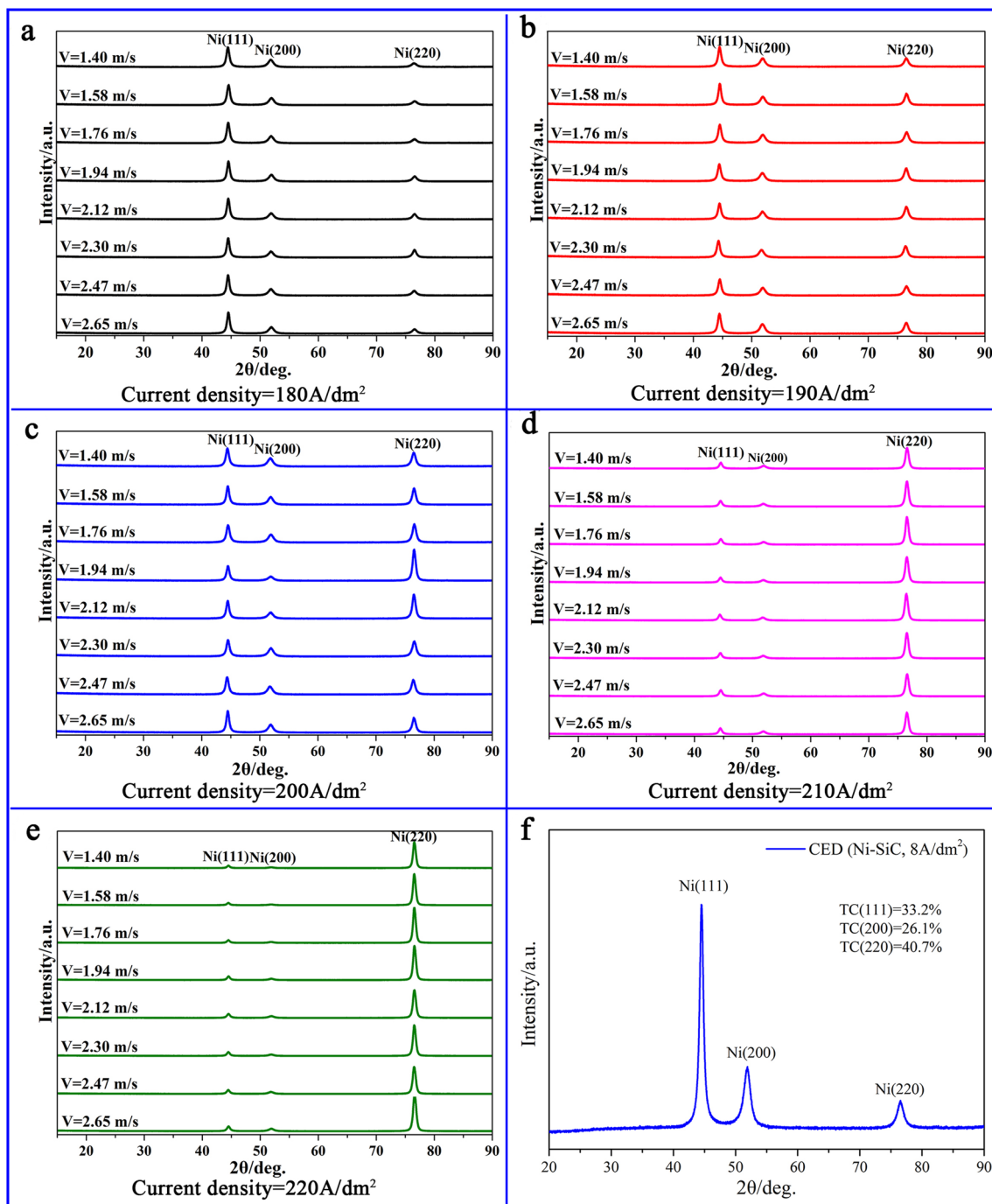


Figure 3 a–e XRD patterns of Ni-SiC composite coatings prepared using JED under different deposition parameters, and **f** XRD pattern of Ni-SiC composite coating prepared using CED

based on the deposition current density according to the Tafel formula. Under the condition of a low deposition current density, the grain orientation of coating tends to be (111). As the deposition current density increases the grain orientation of the coating gradually evolves to

(220). When the deposition current density exceeds a certain value, most of the cells are adsorbed on the substrate with the (220) crystalline plane.

Compared with the influence of the deposition current density, the effect of the injection velocity on the grain

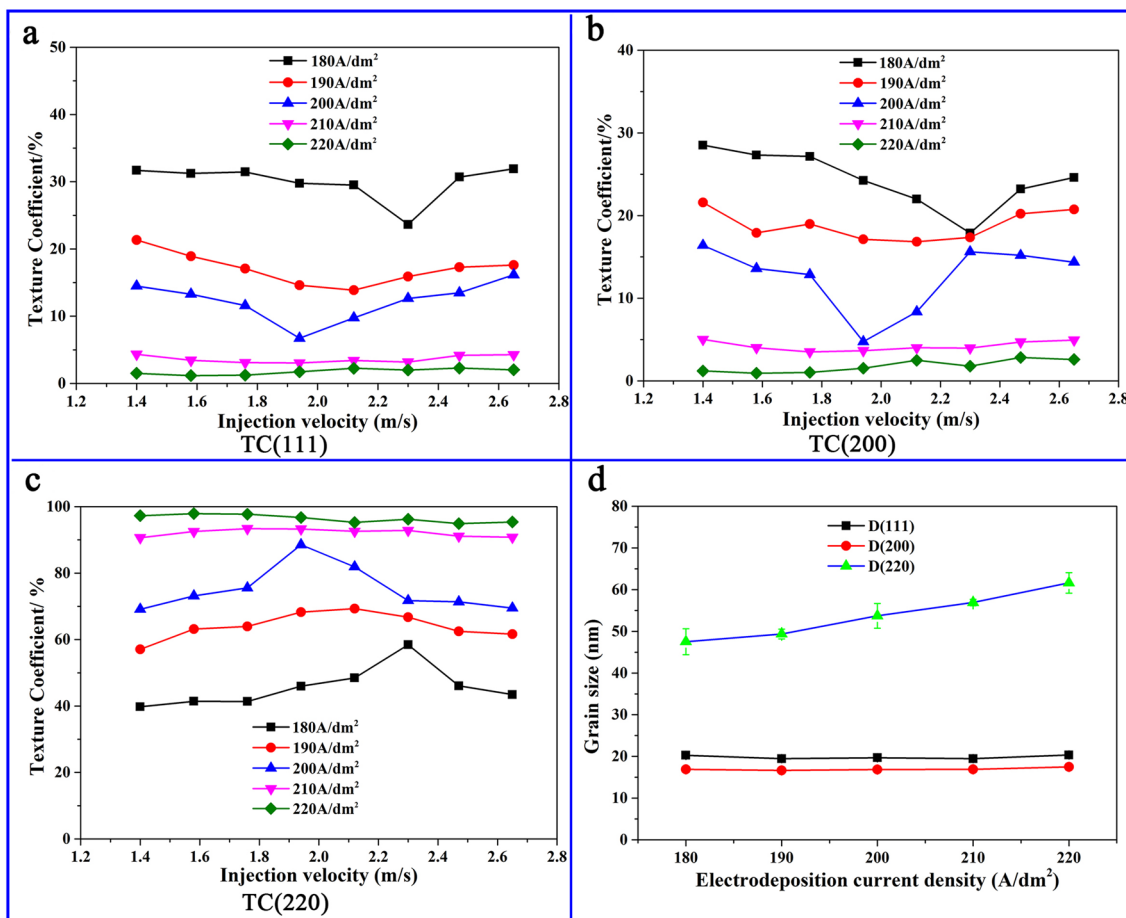


Figure 4 a–c The texture coefficients of Ni-SiC composite coatings prepared using JED under different deposition parameters: **a** TC(111), **b** TC(200), and **c** TC(220); **d** The grain size statistic of Ni-SiC composite coatings prepared using JED under different deposition parameters

orientation of the coating is smaller. Because the bonding strength of the (111) - and (200) - oriented grains to the substrate is less than that of the (220) - oriented grains, the increase in the injection velocity tends to makes the nickel structure cells adsorb into the substrate with the (220) crystalline plane. However, the TC(220) of the coating does not increase monotonically with an increase in the injection velocity. There is a critical value for the injection speed. When the injection speed exceeds this value, the nickel structure cells tend to adsorb into the substrate with random crystalline planes instead. The critical value has a negative correlation with the density of deposition current, that is, the smaller the deposition current density is, the larger the critical value.

Under the condition of a high deposition current density, the nickel structure cells rapidly nucleate, and the number of crystal nuclei with a (220) orientation is larger than that with (111) and (200) orientations. Therefore, the crystal nucleus with the (220) orientation dominates the growth process. Eventually, the average size of the

(220) orientation grains is clearly larger than that of the (111) and (200) orientation grains.

3.2 Morphology of Ni-SiC Composite Coating with Highly Preferred (220) Orientation

Figure 6 shows the morphology of a Ni-SiC composite coating with a highly preferred (220) orientation prepared using JED (TC(220) = 97.7%). As shown in Figure 6a, the surface (Area C) and section (Area F) of the coating were observed. It is clear that the surface of the Ni SiC composite coating with a highly preferred (220) orientation is compact and flat (Figure 6c, f), and there is no dome or hill/ valley-like structure [16, 23–25]. The surface roughness of the coating was R_a 0.119 μm (Figure 6b). SiC nanoparticles had no agglomeration inside the coating (Figure 6d, g) and were evenly distributed in different areas of the coating (Figure 6e, h).

Figure 7 shows the morphology of a Ni-SiC composite coating without a highly preferred (220) orientation prepared using JED (TC(220) = 41.4%). As shown in

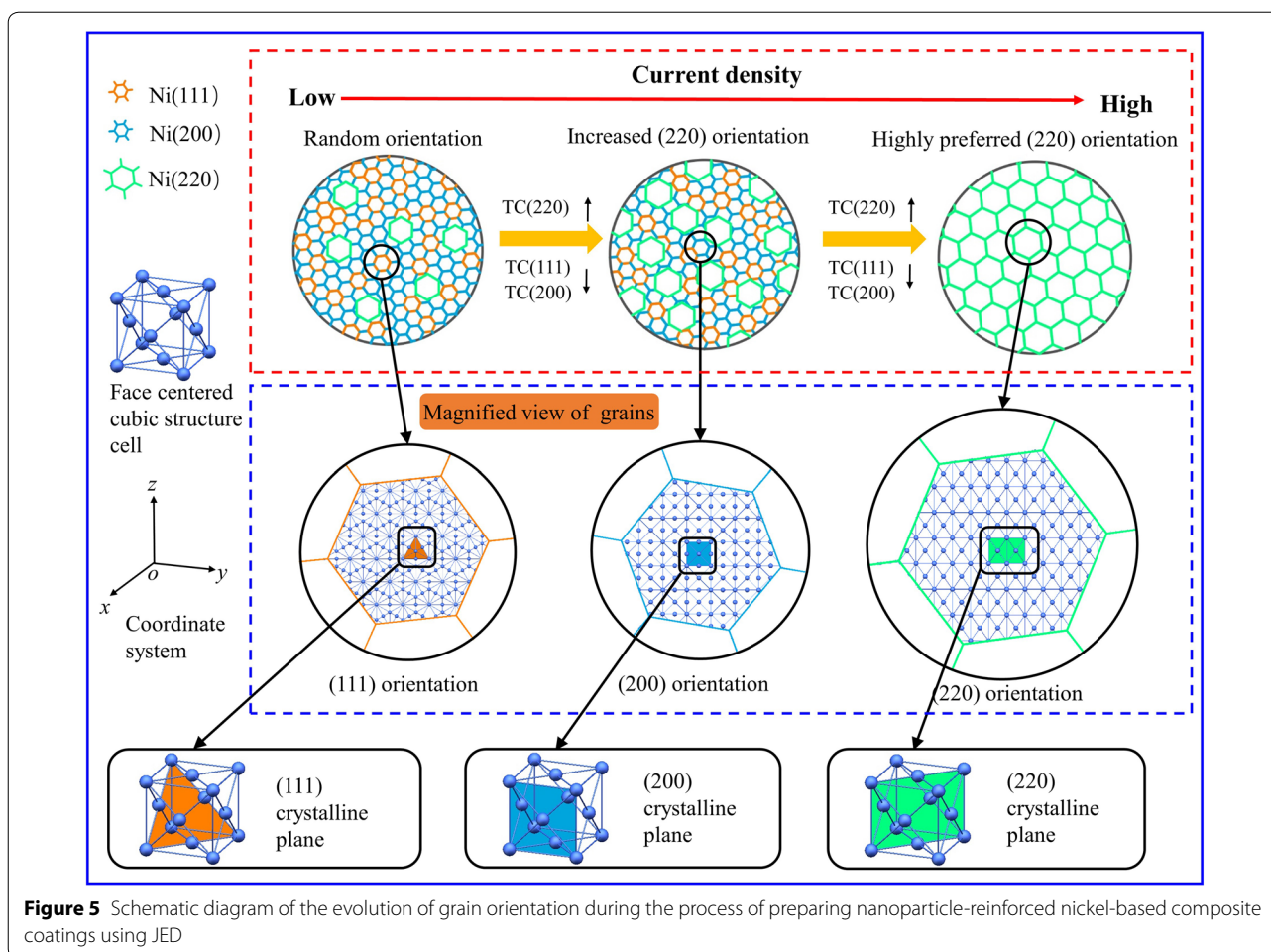


Figure 5 Schematic diagram of the evolution of grain orientation during the process of preparing nanoparticle-reinforced nickel-based composite coatings using JED

Figure 7a, the surface (Area C) and section (Area F) of the coating were observed. It is clear that the surface of the Ni SiC composite coating has slight bumps and gullies. The surface roughness of the coating was R_a 0.321 μm (Figure 7b). SiC nanoparticles have no agglomeration inside the coating (Figure 7d, g) and were evenly distributed in different areas of the coating (Figure 7e, h).

Figure 8 shows the morphology of a Ni-SiC composite coating prepared using CED (TC(220) = 40.7%). As shown in Figure 8a, the surface (Area C) and section (Area F) of the coating were also observed. The surface of the Ni SiC composite coating prepared by CED is coarse and fluctuant (Figure 8c, f). The surface roughness of the coating was R_a 1.210 μm (Figure 8b). SiC nanoparticles have an obvious agglomeration inside the coating (Figure 8d, g) and the content varies greatly in different areas (Figure 8e, h).

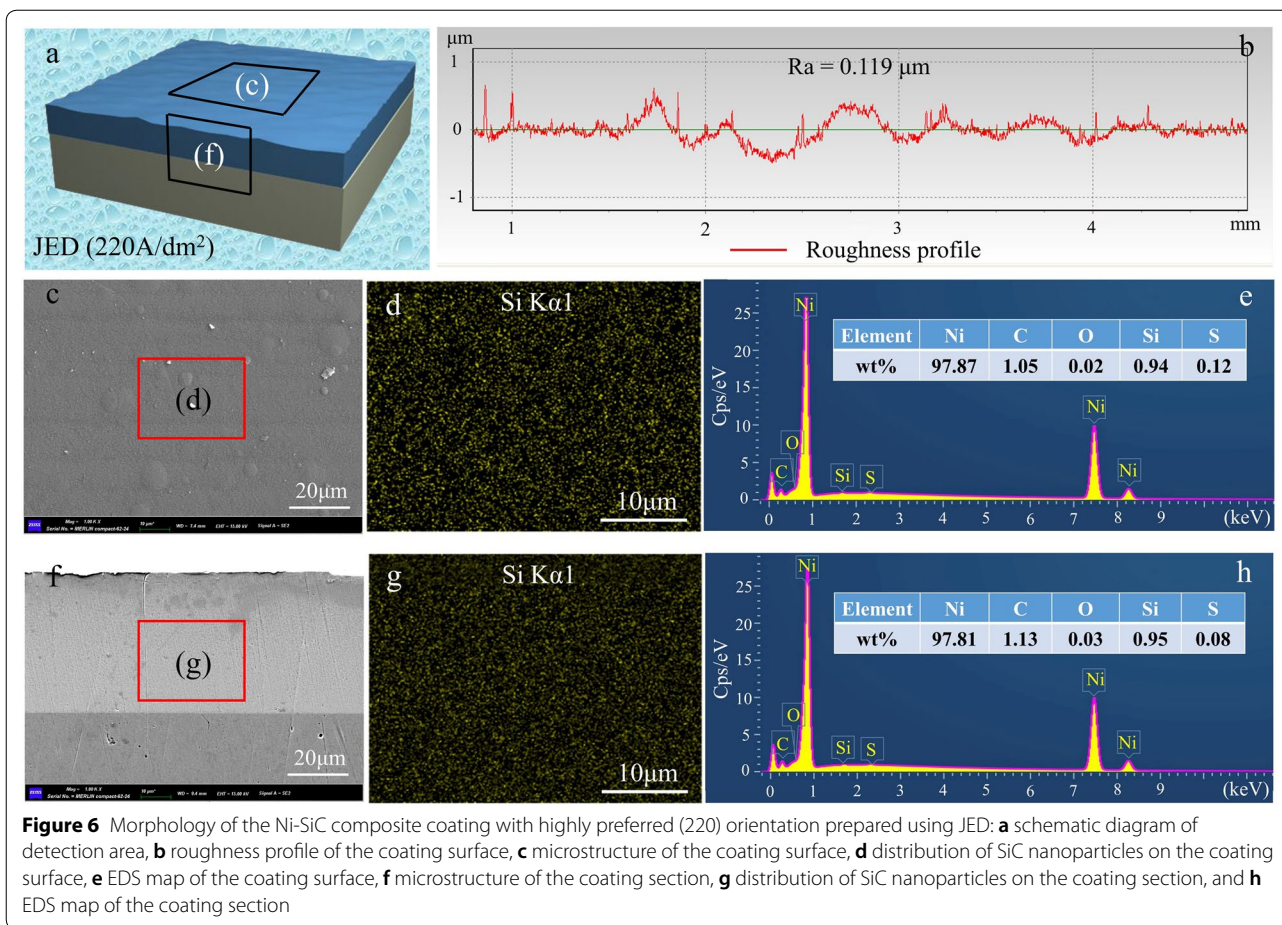
Compared with the coating prepared using CED, The high-speed jetting process used by JED can make SiC nanoparticles evenly distributed in the coating and the surface quality of the coating prepared through JED is

obviously improved owing to the high-speed scouring of the plating solution. For the JED, the Ni-SiC composite coating with a highly preferred (220) orientation has a smoother surface topography, which is beneficial for significantly improve the corrosion resistance of the Ni-SiC composite coating.

3.3 Corrosion Resistance of Ni-SiC Composite Coating with Highly Preferred (220) Orientation

In this study, the corrosion resistance of the Ni-SiC composite coating was tested, including electrochemical tests and full immersion corrosion tests. Figure 9 shows the electrochemical test results of the Ni-SiC composite coatings in a 3.5 wt% NaCl solution. The dynamic polarization curves are shown in Figure 9a. As can be seen from this figure, the corrosion potential (E_{corr}) and corrosion current density (i_{corr}) of the Ni-SiC composite coating prepared using CED were -0.747 V and 54.52 $\mu\text{A}/\text{cm}^2$, respectively.

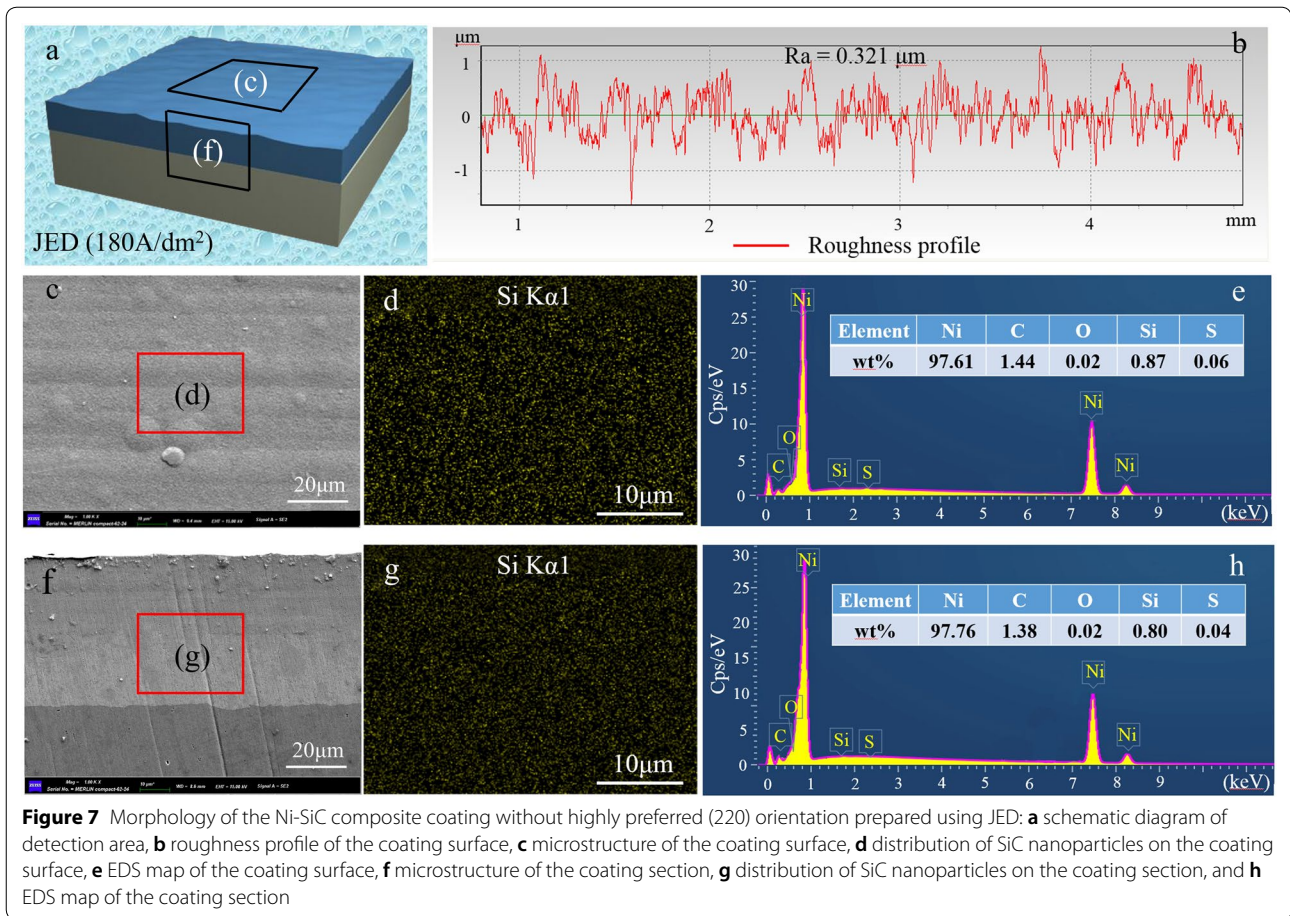
The Ni-SiC composite coatings were prepared using JED at an injection velocity of 1.76 m/s and a



current density of 180–220 A/dm². With an increase in the deposition current density, the TC(220) of the coating increases from 41.4% to 97.7%, the corrosion potential of the coating increased from -0.575 to -0.477 V, and the corrosion current density decreased from 9.52 to 2.76 μA/cm². This indicates that the corrosion resistance of the coating was enhanced. EIS is a powerful and nondestructive electrochemical technology to confirm electrochemical reactions and study the corrosion behavior of electrode/electrolyte interface [26–29]. Figure 9b shows the typical Nyquist plots of the Ni-SiC composite coatings. A depressive semicircle can be found on each curve, indicating that the electrochemical mechanism is controlled by the charge-transfer process [30]. It can be seen that the diameter of the capacitive loop increases with an increase in TC(220) of the Ni-SiC composite coating. A larger diameter of the capacitive loop, results in a stronger corrosion resistance of the coating. Figure 9c shows the Bode plots of log(f) versus log(|Z|) of the Ni-SiC composite coatings. Within the high-frequency region (10⁴ to 10⁵ Hz), the values of log|Z| are similar, indicating that these are impedance values of a

3.5 wt% NaCl solution. Within the low-frequency region (10⁻² to 10⁻¹ Hz), the impedance values of the different Ni-SiC composite coatings are significantly different. For instance, at a fixed 0.01 Hz, the log(|Z|) of the Ni-SiC composite coating prepared using CED is 3.41, and the log(|Z|) of Ni-SiC composite coating prepared by JED increase from 3.99 to 4.72 as TC(220) increase from 41.4% to 97.7%. The higher the impedance value is, the stronger the corrosion resistance of the coating. Figure 9d shows the Bode plots of log(f) versus angle of the Ni-SiC composite coatings. For the Ni-SiC composite coatings, the higher phase angle at the middle high frequency for the chemical-conversion-treated specimen corresponds to a capacitive behavior, that is, the conversion coating has good dielectric properties to avoid the ionic flow of the electrolyte [30]. When the frequency is in the range of 10⁰ to 10⁵ Hz, the phase angle of the Ni-SiC composite coating prepared using CED is minimum, and the phase angle of the Ni-SiC composite coating prepared using JED increases with an increase in TC(220).

The EIS data were fitted using an electrical equivalent circuit (EEC). The corrosion process of the Ni-SiC



composite coating can be replaced with the EEC of $R(Q(R(QR)))$ when the oxide layer on the substrate surface is taken into account [31].

As observed in Figure 9e, the EEC consists of the R_s modeling of the solution resistance, in sequence with a constant phase element CPE_1 in parallel with another resistance R_c modeling the coating resistance, followed by another constant phase element CPE_2 and a third charge transfer resistance of R_{ct} associated with the corrosion process. The impedance of the CPE is defined through Eq. (3):

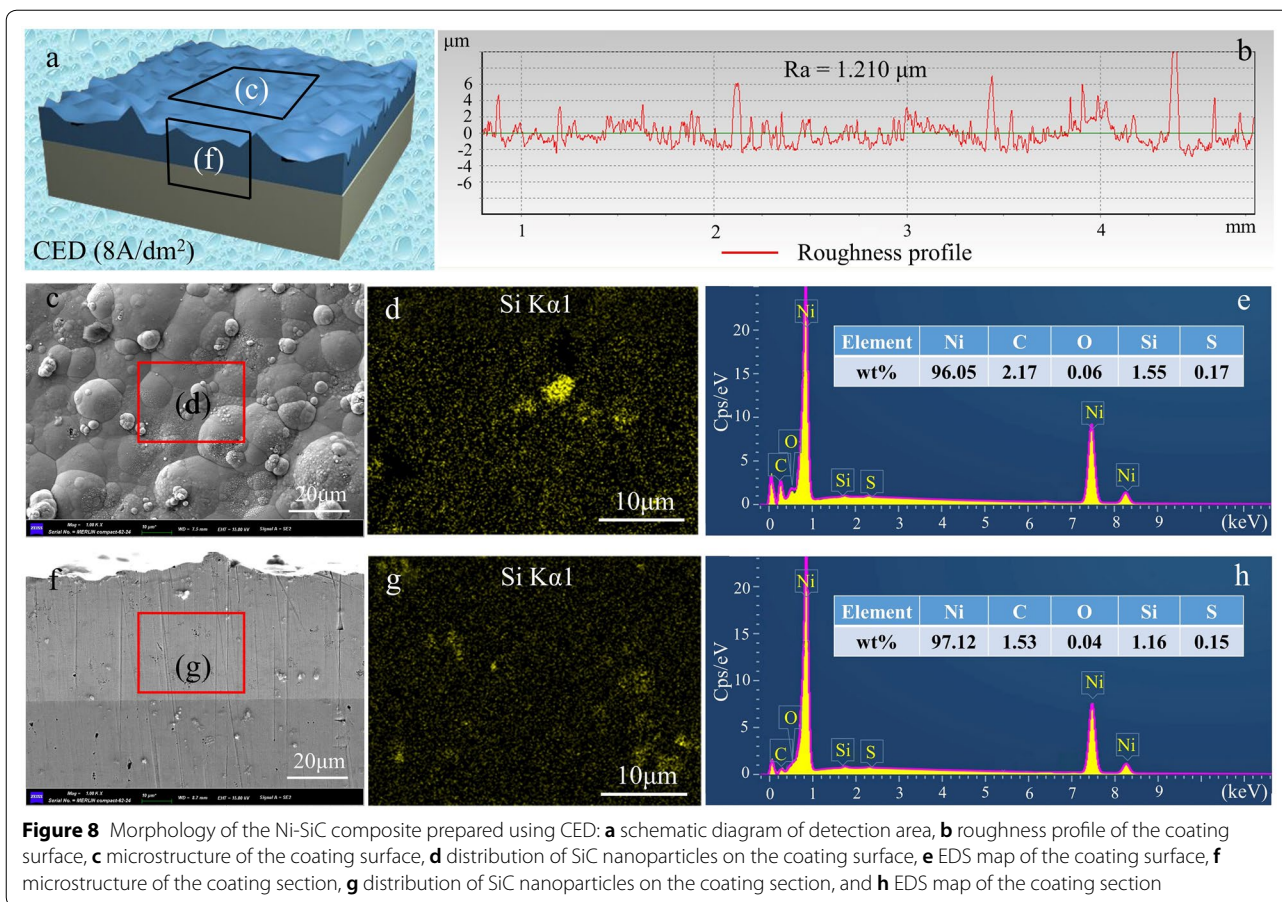
$$Q_{CPE} = [Y_0(j\omega)^n]^{-1}, \tag{3}$$

where ω is the angular frequency (rad/s), Y_0 is the CPE admittance, j is the imaginary number ($\sqrt{-1}$), and n with a value of 0–1 represents the relaxation dispersion. When $n = 1$, the CPE is a pure capacitor with a capacitance of Y_0 . It is believed that the smaller the n value is, the more defects that will occur on the surface and the more likely pitting corrosion is to occur [30, 32].

The fitting results are listed in Table 2. It can be seen that R_c and R_{ct} of the Ni-SiC composite coating prepared using CED are $1.476 \times 10^2 \Omega \cdot \text{cm}^2$ and $3.846 \times 10^3 \Omega \cdot \text{cm}^2$, respectively. Compared with that of other coatings, these parameters are the minimum values, which means that this coating has the worst corrosion resistance. The Ni-SiC composite coatings prepared using JED with TC(220) increased from 41.4% to 97.7%, the R_c of the coatings increased from 4.423×10^3 to $7.025 \times 10^3 \Omega \cdot \text{cm}^2$, and the R_{ct} increased from 1.267×10^4 to $5.989 \times 10^4 \Omega \cdot \text{cm}^2$. It was proved that the corrosion resistance of the Ni-SiC composite coating increased with an increase in TC(220).

The central area of the coatings after immersion corrosion is observed, and the surface morphologies of different corrosion times are shown in Figures 10, 11, 12 and 13.

It is obvious that when the corrosion time is 1, 3, or 5 days, the central area of the different coatings was mostly unchanged, indicating that the corrosion did not extend to the central area. When the corrosion time was 10 days,



corrosion pits of different sizes appeared on the central surface of the coatings. Figure 13a shows the surface morphology of the Ni-SiC composite coating prepared using CED after 10 days of immersion corrosion. It can be seen that many corrosion products adhere to the surface of the coating, and the size of the corrosion pits is approximately 3.3–22.2 μm. Figure 13b–f are the surface morphologies of Ni-SiC composite coatings prepared using JED after 10 days of immersion corrosion. Compared with Figure 13a, there are no obvious corrosion products on the surface of the coating, and the corrosion pits are all less than 1 μm. When the TC(220) of the coating was 41.4%, the size of the corrosion pits was approximately 278–944 nm (Figure 13b). When the TC(220) of the coating was 63.9%, the size of the corrosion pits was approximately 254–927 nm (Figure 13c). When the TC(220) of the coating was 75.6%, the size of the corrosion pits was approximately 215–905 nm (Figure 13d). When the TC(220) of the coating was 93.4%, the size of the corrosion pits was approximately 183–352 nm (Figure 13e). Finally, when the TC(220) of the coating was 97.7%, the size of the corrosion pits was approximately 153–260 nm (Figure 13f). This shows that as the TC(220)

increases, the corrosion resistance of the Ni-SiC composite coating is improved.

The surface quality is the most important factor affecting the corrosion resistance of the coating. The corrosion resistance of the coating decreases with an increase in the number of surface defects. There are many defects on the surface of Ni-SiC composite coating prepared using CED, such as the agglomeration of the SiC nanoparticles, pinholes and pockmarks. Corrosion occurs preferentially at these defect locations, and over a period of time, it is easy to cause SiC agglomerated particles to fall off, resulting in the formation of holes in the coating, which eventually form larger corrosion pits with the increase in corrosion time. The surfaces of the Ni-SiC composite coatings prepared using JED are compact and flat without obvious defects and SiC particle agglomeration; thus, the corrosion resistance of the coatings is significantly improved. The corrosion pits occur uniformly at the grain boundaries on the coating surface, and the corrosion pits gradually expand with the increase in corrosion time. Under the same corrosion area, the smaller the grain boundary proportion and the smaller the number

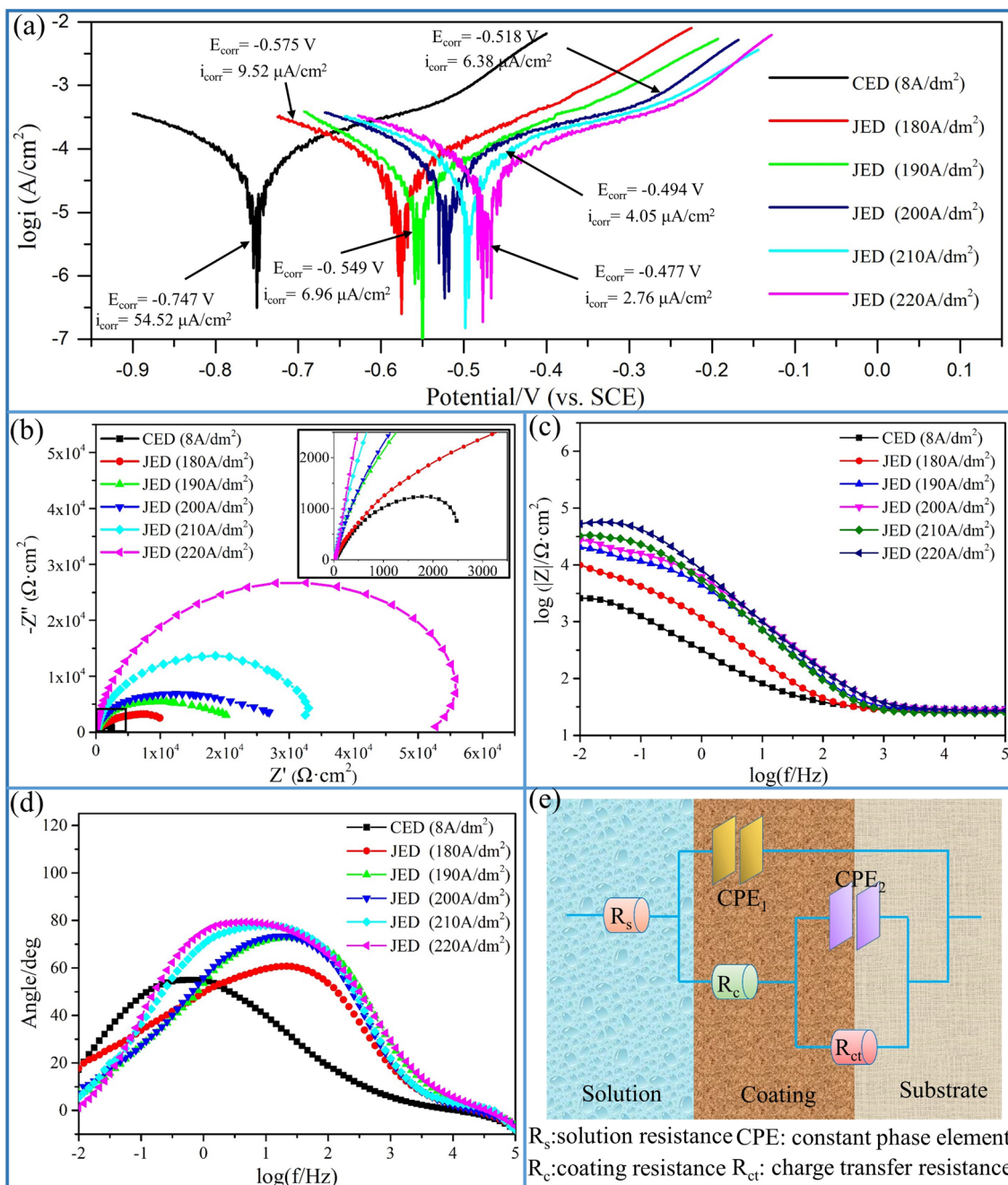


Figure 9 Electrochemical test results of Ni-SiC composite coatings: **a** dynamic polarization curves, **b** Nyquist plots, **c** Bode plots of $\log(f)$ versus $\log(|Z|)$, **d** Bode plots of $\log(f)$ versus the angle, and **e** schematic diagram of the EEC

of corrosion pits. As the deposition current density increased, the grain size of the Ni-SiC composite coating also increased, and the proportion of grain boundaries decreased. At the same time, with the increase in TC(220), the coating with the same orientation

gradually formed. The dislocations and other defects at the grain boundaries also reduced and the diffusion rate of corrosion pits is reduced. Therefore, the Ni-SiC coating with a highly preferred (220) orientation shows an excellent corrosion resistance.

Table 2 Parameters fitted from EEC

Preparation method	TC(220) (%)	R_s ($\Omega \cdot \text{cm}^2$)	CPE_1		R_c ($\Omega \cdot \text{cm}^2$)	CPE_2		R_{ct} ($\Omega \cdot \text{cm}^2$)
			Y_1 ($\text{S} \cdot \text{cm}^{-2} \cdot \text{s}^n$)	n_1		Y_2 ($\text{S} \cdot \text{cm}^{-2} \cdot \text{s}^n$)	n_1	
CED (8 A/dm ²)	40.7	28.37	8.579×10^{-4}	0.6753	1.476×10^2	8.759×10^{-4}	0.6846	3.846×10^3
JED (180 A/dm ²)	41.4	25.83	1.661×10^{-4}	0.5643	4.423×10^3	1.658×10^{-4}	0.5635	1.267×10^4
JED (190 A/dm ²)	63.9	28.32	3.686×10^{-5}	0.8795	1.159×10^3	4.880×10^{-5}	0.5677	2.119×10^4
JED (200 A/dm ²)	75.6	28.83	2.588×10^{-5}	0.8722	1.571×10^3	3.386×10^{-4}	0.6184	2.608×10^4
JED (210 A/dm ²)	93.4	24.97	3.543×10^{-5}	0.8938	2.309×10^3	2.463×10^{-5}	0.7570	3.499×10^4
JED (220 A/dm ²)	97.7	28.04	6.916×10^{-6}	0.8984	7.025×10^3	1.566×10^{-5}	0.8623	5.989×10^4

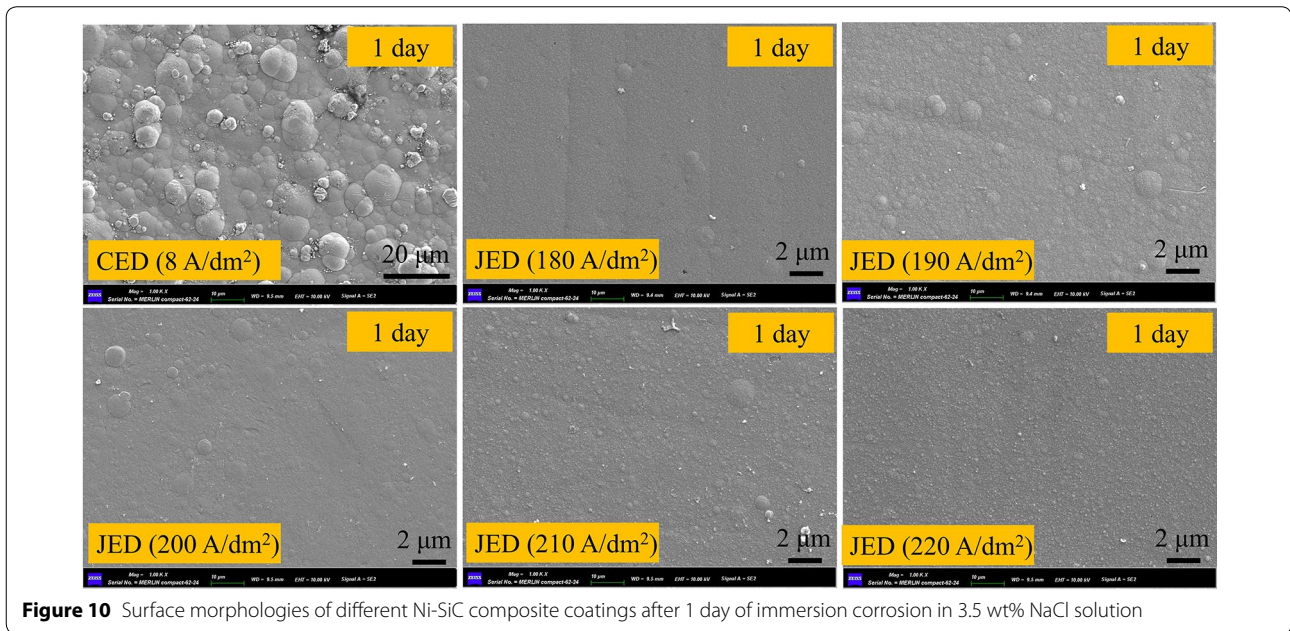


Figure 10 Surface morphologies of different Ni-SiC composite coatings after 1 day of immersion corrosion in 3.5 wt% NaCl solution

3.4 Adhesion Force of Ni-SiC Composite Coating with Highly Preferred (220) Orientation

The adhesion force is an important index for judging the performance of the coating. The higher the adhesion force of the coating, the less easy it is for the coating to fall off, and the longer the service life will be. In this study, the adhesion of the Ni-SiC composite coatings and substrate is quantitatively measured using a scratch method. Figure 14a shows the scratch morphology of the Ni-SiC composite coating prepared using CED, and Figure 14b–f show the scratch morphologies of the Ni-SiC composite coatings prepared using JED under the deposition current density of 180–220 A/dm². As shown in the elliptical frame selection area, the load corresponding to the first crack position of the coating is defined as the value of the adhesion force, which is 20.5, 24.9, 46.8, 55.2, 60.5, and 61.6 N, respectively. It can be seen that the

adhesion force of the Ni-SiC composite coating has a positive correlation with the TC(220) value. The higher the TC(220) is, the higher the adhesion force of the coating.

From a microscopic perspective, the adhesion force between the coating and substrate depends on the contact strength of the interface. A fundamental quantity determining the strength of the interface is the ideal work of the adhesion (W_{ad}), which is the work spent on separating the interface into two free surface. The work of adhesion between the coating and substrate can be calculated using Eq. (4) [33, 34]:

$$W_{ad} = (E_{slab1} + E_{slab2} - E_{int})/A, \tag{4}$$

where E_{slab1} and E_{slab2} are the total energies of slab1 and slab2, E_{int} is the total energy of the interface system including slab1 and slab2, and A is the interface area.

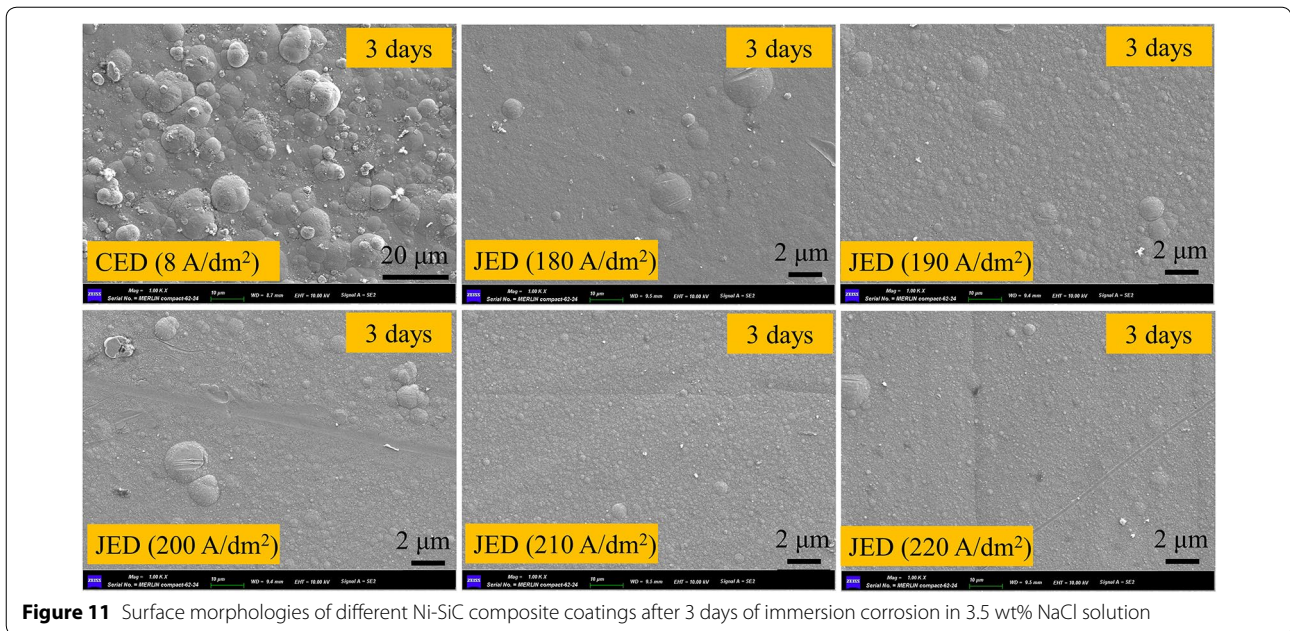


Figure 11 Surface morphologies of different Ni-SiC composite coatings after 3 days of immersion corrosion in 3.5 wt% NaCl solution

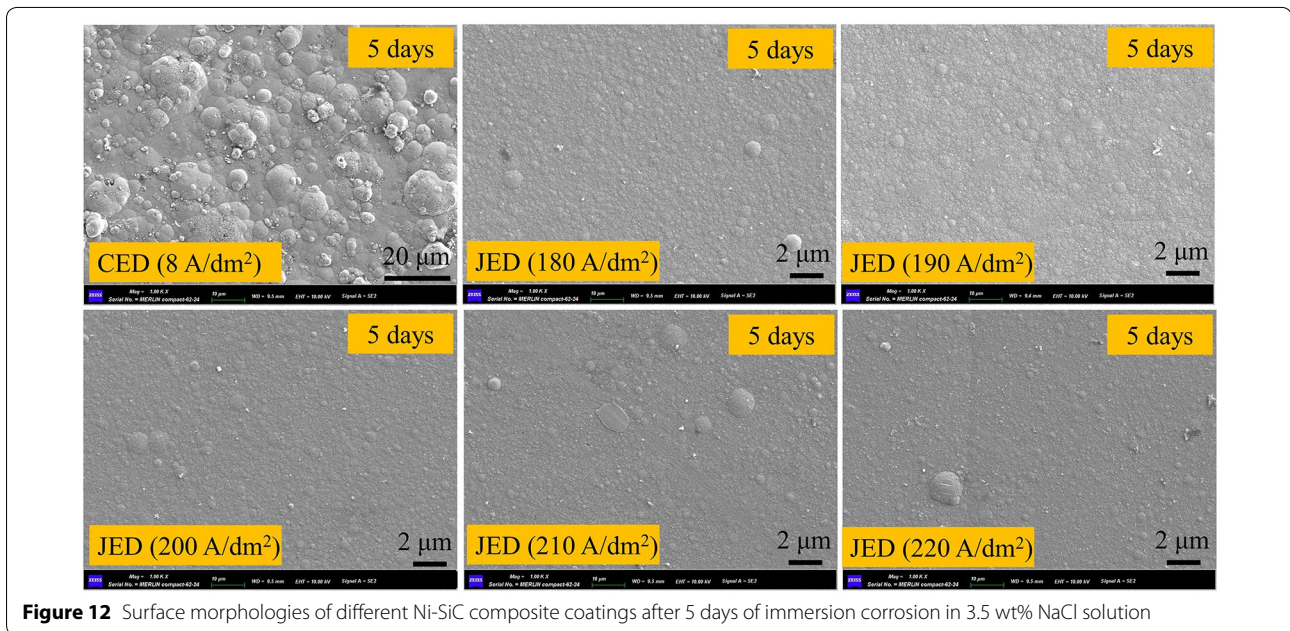


Figure 12 Surface morphologies of different Ni-SiC composite coatings after 5 days of immersion corrosion in 3.5 wt% NaCl solution

The DFT simulation models are shown in Figure 15. The substrate is medium-carbon steel, and the main orientation of the substrate is Fe(110). The W_{ad} values of the Ni(111)/Fe(110), Ni(200)/Fe(110), and Ni(220)/Fe(110) interfaces are 3.32, 3.96, and 4.21 J/m², respectively. The

W_{ad} value of the Ni(220)/Fe(110) interface is greater than that of the Ni(111)/Fe(110) interface and Ni(200)/Fe(110) interface, indicating that the adhesion force between the Ni-SiC composite coating with a highly preferred (220) orientation and substrate is higher.

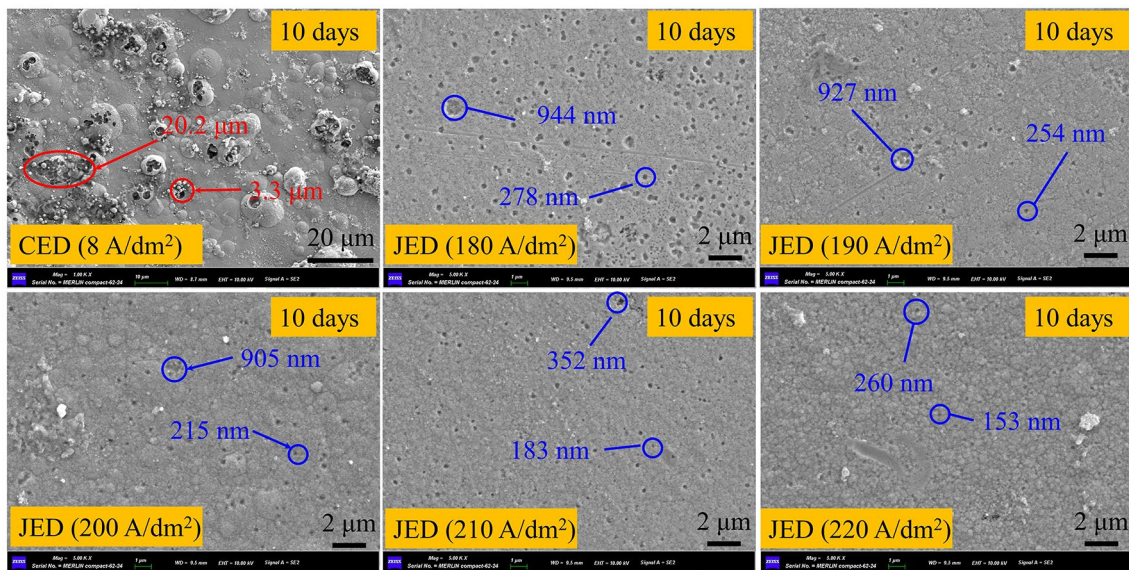


Figure 13 Surface morphologies of different Ni-SiC composite coatings after 10 days of immersion corrosion in 3.5 wt% NaCl solution

4 Conclusions

(1) The grain orientation of the Ni-SiC composite coatings prepared using JED gradually evolves into (220) with an increase in the current density. The Ni-SiC composite coating with a highly preferred (220) orientation was prepared at a current density of 220 A/dm², whereas the orientation coefficient reached 97.7%.

(2) During the JED process, the high-speed jetting fluid causes the nanoparticles to break the agglomeration state and disperse evenly into the coating. Under the condition of a high current density, the deposition layer quickly fills the defects of the substrate and forms a compact and flat composite coating on the surface. The surface roughness of the Ni-SiC composite coating with a highly preferred (220) orientation is 90.2% lower than that of the Ni-SiC composite coating prepared using CED.

(3) The corrosion resistance of the Ni-SiC composite coatings increases with an increase in TC(220). Compared with the corrosion resistance of the coating prepared using CED, the corrosion resistance of the coating with the highly preferred (220) orientation prepared using JED has a 36.1% increase in corrosion potential and a 94.9% decrease in corrosion current density.

(4) A DFT simulation was conducted to calculate the ideal work of adhesion of the Ni(111)/Fe(110), Ni(200)/Fe(110), and Ni(220)/Fe(110) interfaces of the Ni-SiC composite coating, among which the Ni(220)/Fe(110) interface has a higher Wad than the Ni(111)/Fe(110) and Ni(200)/Fe(110) interfaces. The Ni-SiC composite coating with a highly preferred (220) orientation obtains the maximum adhesion force, which is 200% higher than that of the Ni-SiC composite coating prepared using CED.

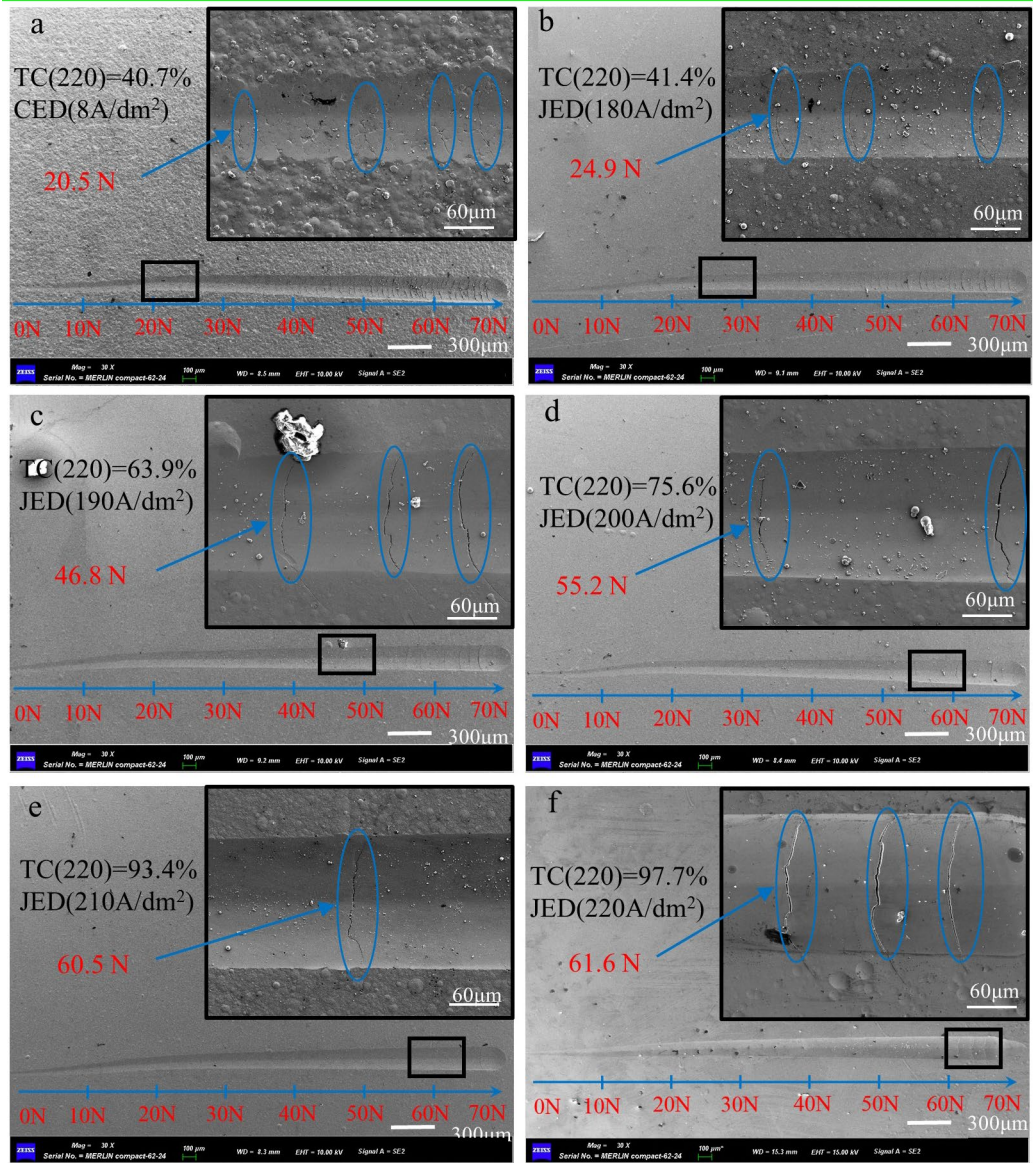


Figure 14 (a–f) Scratch morphology of different Ni-SiC composite coatings: **a** CED (8 A/dm²), **b** JED (180 A/dm²), **c** JED (190 A/dm²), **d** JED (200 A/dm²), **e** JED (210 A/dm²), **f** JED (220 A/dm²)

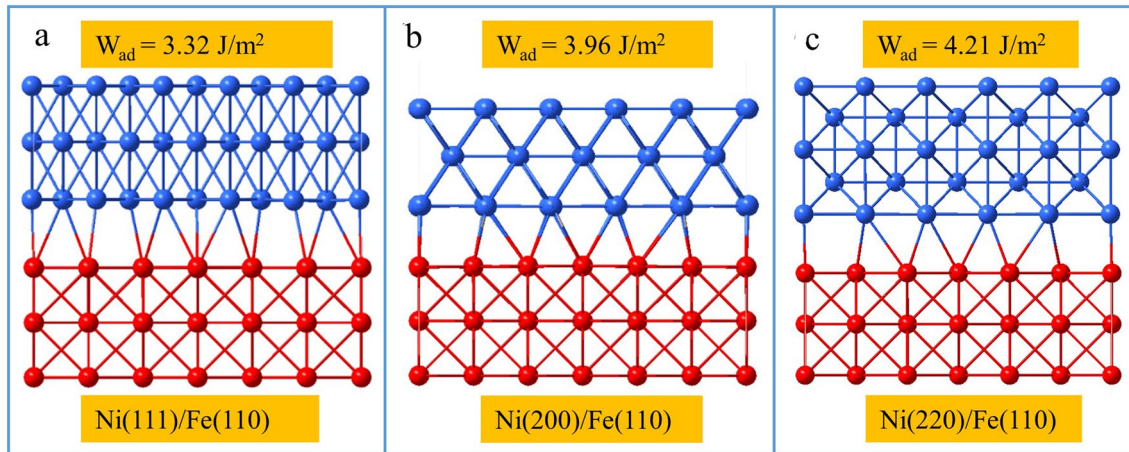


Figure 15 DFT optimized structures of **a** Ni(111)/Fe(110), **b** Ni(200)/Fe(110) and **c** Ni(220)/Fe(110) interfaces

Acknowledgements

Not applicable.

Authors' Contributions

RJ and HJ contributed equally. The manuscript was written by RJ, YL and HJ. Experiments were designed by TD, FZ, LZ and CM. XW, QS, HD, DL, PL and BC performed the experiments. All authors have approved the final version of the manuscript.

Authors' Information

Renjie Ji received his PhD degree in Mechanical and Electronic Engineering from *China University of Petroleum* in 2011. He is currently a professor at *China University of Petroleum*, the "Hong Kong Scholar" visiting researcher of *Hong Kong Polytechnic University*. He is the council member of the *Chinese Nontraditional Machining Society*, the vice director of *Youth Committee of Chinese Nontraditional Machining Society* and the member of National Technical Committees 161 on Nontraditional Machine Tools of Standardization Administration of China. His research interest focuses on technology and theory of nontraditional machining.

Hui Jin, born in 1994, received his bachelor's degree of mechanical engineering from *China University of Petroleum (East China)* in 2016, and now working towards his PhD at *China University of Petroleum (East China)*. His research interests include the jet electrodeposition technology and material surface strengthening technology.

Yonghong Liu received his Ph.D. degree in Mechanical Design, Manufacturing and Automation from the *Harbin Institute of Technology, China*, in 1996. He is currently a professor at *China University of Petroleum*, where he is also the Dean of *College of Mechanical and Electronic Engineering*. He enjoys special government allowances issued by the State Council. His research interests include the development of subsea engineering equipment, manufacturing technology of offshore equipment and fault diagnosis methodology.

Tiancong Dong, born in 1997, is currently a master candidate at *Mechanism Laboratory of Mechanical Engineering, China University of Petroleum*. He received his bachelor's degree from *China University of Petroleum, China*, in 2019. His research interests include jet electrodeposition and Electrochemical behavior of coatings.

Fan Zhang, born in 1991, is currently a PhD candidate in Prof. Renjie Ji's group at *College of Mechanical and Electronic Engineering, China University of Petroleum (East China)*. His research interest focuses on the electrochemical energy conversion and storage using transitional metal-based catalysts.

Lilong Zhao awarded a master's degree of Mechanical Engineering (smart product design) from *Nanyang Technological University Singapore* in 2016. He used to be a mechanical design engineer in MCE Singapore and mechatronics engineer in *ALPS-Tech China*. Currently, he is a PhD candidate major in mechanical engineering at *China University of Petroleum*. The main research fields are intelligent manufacturing, electrical discharge machining, robot technology and ergonomics.

Xinlei Wu received his B.S. degree in Mechanical Design & Manufacture and Automation from *China University of Petroleum (East China)* in 2015. He is currently working toward a Ph.D. degree in Mechanical Engineering under the supervision of Prof. Yonghong Liu. His present research interests mainly focus on nontraditional machining, intelligent manufacturing and machine learning.

Qiang Sun, born in 1990, is currently a PhD candidate at *College of Mechanical and Electronic Engineering, China University of Petroleum (East China)*. His research interests include plasma drilling direction and plasma cutting technology.

Peng Liu received his PhD degree from *China University of Petroleum (East China)* in 2020. His recent research interests include reliability engineering, fault diagnosis, and Bayesian network methodology and application. E-mail: liupeng@s.upc.edu.cn.

Hang Dong received his PhD degree from *China University of Petroleum (East China)* in 2020. His recent research include nontraditional machining, and advanced manufacturing technology.

Chi Ma, born in 1994, is currently a PhD candidate at *College of Mechanical and Electronic Engineering, China University of Petroleum (East China)*, China. He received his bachelor's degree from *China University of Petroleum (East China)*, China, in 2017. His research interests include additive manufacturing and control.

Dege Li, born in 1993, received his bachelor's degree in mechanical engineering from *China University of Petroleum (East China)* in 2016, and now working towards his PhD at *China University of Petroleum (East China)*. His research interests include the fabrication of microfluidic systems, ultra-fine droplet generation and manipulation, and satellite droplet mechanisms.

Baoping Cai received his BS degree in Mechanical Design, Manufacturing and Automation from the *China University of Petroleum* in 2006. He received his Ph.D. degree in Mechanical and Electronic Engineering from *China University of Petroleum* in 2012. He is a lecturer at the same university from 2013 to 2014. Currently, he is a professor at the *China University of Petroleum*. His research

interests include reliability engineering, fault diagnosis, risk analysis, and Bayesian network methodology and application.

Funding

Supported by National Natural Science Foundation of China (Grant No. 51675535), Major Research Project of Shandong Province of China (Grant No. 2019GGX104068), Key Pre-Research Foundation of Military Equipment of China (Grant No. 6140923030702), National Science and Technology Major Project of China (Grant No. 2017ZX05072), Graduate Innovation Project of China University of Petroleum (East China) (Grant No. YCX2020059) and Science and Technology Support Plan for Youth Innovation of Universities in Shandong Province of China (Grant No. 2019KJB016).

Competing interests

The authors declare no competing financial interests.

Author Details

¹ College of Mechanical and Electronic Engineering, China University of Petroleum (East China), Qingdao 266580, China. ² Key Laboratory of Unconventional Oil & Gas Development, Ministry of Education, China University of Petroleum (East China), Qingdao 266580, China.

Received: 25 April 2020 Revised: 16 September 2020 Accepted: 10 November 2020
Published online: 03 December 2020

References

- R Li, Y Hou, B Liu, et al. Electrodeposition of homogenous Ni/SiO₂ nano-composite coatings from deep eutectic solvent with in-situ synthesized SiO₂ nanoparticles. *Electrochimica Acta*, 2016, 222: 1272-1280.
- B Li, D Li, W Chen, et al. Effect of current density and deposition time on microstructure and corrosion resistance of Ni-W/TiN nanocomposite coating. *Ceramics International*, 2019, 45(4): 4870-4879.
- Y Tao, F Ma, M Teng, et al. Designed fabrication of super high hardness Ni-B-Sc nanocomposite coating for anti-wear application. *Applied Surface Science*, 2019, 492: 426-434.
- M Alizadeh, A Cheshmpish. Electrodeposition of Ni-Mo/Al₂O₃ nano-composite coatings at various deposition current densities. *Applied Surface Science*, 2019, 466: 433-440.
- S Banthia, S Sengupta, S Das, et al. Synthesis and characterization of novel Cu, Cu-SiC functionally graded coating by pulse reverse electrodeposition. *Applied Surface Science*, 2019, 467-468: 567-579.
- C Wang, L Shen, M Qiu, et al. Characterizations of Ni-CeO₂ nanocomposite coating by interlaced jet electrodeposition. *Journal of Alloys and Compounds*, 2017, 727: 269-277.
- C Ma, W Yu, M Jiang, et al. Jet pulse electrodeposition and characterization of Ni-AlN nanocoatings in presence of ultrasound. *Ceramics International*, 2018, 44(5): 5163-5170.
- W Jiang, L Shen, M Qiu, et al. Preparation of Ni-SiC composite coatings by magnetic field-enhanced jet electrodeposition. *Journal of Alloys and Compounds*, 2018, 762: 115-124.
- W Cui, K Wang, F Xia, et al. Simulation and characterization of Ni-doped SiC nanocoatings prepared by jet electrodeposition. *Ceramics International*, 2018, 44(5): 5500-5505.
- F F Xia, W C Jia, C Y Ma, et al. Synthesis and characterization of Ni-doped TiN thin films deposited by jet electrodeposition. *Applied Surface Science*, 2018, 434: 228-233.
- H Gao, W Zhen, J Ma, et al. High efficient solar hydrogen generation by modulation of Co-Ni sulfide (220) surface structure and adjusting adsorption hydrogen energy. *Applied Catalysis B: Environmental*, 2017, 206: 353-363.
- A Ponrouch, S Garbarino, E Bertin, et al. Highly porous and preferentially oriented {100} platinum nanowires and thin films. *Advanced Functional Materials*, 2012, 22(19): 4172-4181.
- J Kim, K H Lee, S W Kim, et al. Potential-current co-adjusted pulse electrodeposition for highly (110)-oriented Bi₂Te_{3-x}Se_x films. *Journal of Alloys and Compounds*, 2019, 787: 767-771.
- J A Calderón, J E Henao, M A Gómez. Erosion–corrosion resistance of Ni composite coatings with embedded SiC nanoparticles. *Electrochimica Acta*, 2014, 124: 190-198.
- Y Zhao, L Wang, Y Sun, et al. Influences of Al and Ti particles on microstructure, internal stress and property of Ni composite coatings. *Journal of Alloys and Compounds*, 2019, 793: 314-325.
- M Alizadeh, H Safaei. Characterization of Ni-Cu matrix, Al₂O₃ reinforced nano-composite coatings prepared by electrodeposition. *Applied Surface Science*, 2018, 456: 195-203.
- J Deng, J Zhang, Y Tu, et al. Effect of BEO in the electrodeposition process of Ni/diamond composite coatings for preparation of ultra-thin dicing blades: Experiments and theoretical calculations. *Ceramics International*, 2018, 44(14): 16828-16836.
- R Ji, K Han, H Jin, et al. Preparation of Ni-SiC nano-composite coating by rotating magnetic field-assisted electrodeposition. *Journal of Manufacturing Processes*, 2020, 57: 787-797.
- N Guglielmi. Kinetics of the deposition of inert particles from electrolytic baths. *Journal of the Electrochemical Society*, 1972, 119(8): 1009.
- J P Celis, J R Roos, C Buelens. A mathematical model for the electrolytic codeposition of particles with a metallic matrix. *Journal of the Electrochemical Society*, 2019, 134(6): 1402-1408.
- S Xie, M Dai, S Lin, et al. Effect of bias voltage on the oxidation resistance of NiCoCrAlYTa coatings prepared by arc ion plating. *Corrosion Science*, 2019, 147: 330-341.
- X Chen, X Qin, Z Zhu, et al. Microstructural evolution and wear properties of the continual local induction cladding NiCrBSi coatings. *Journal of Materials Processing Technology*, 2018, 262: 257-268.
- Y E Sknar, O O Savchuk, I V Sknar. Characteristics of electrodeposition of Ni and Ni-P alloys from methanesulfonate electrolytes. *Applied Surface Science*, 2017, 423: 340-348.
- S Kumaraguru, G G Kumar, S Shanmugan, et al. Enhanced texture and microhardness of the nickel surface using Bi₂O₃ particles via electrodeposition technique for engineering application. *Journal of Alloys and Compounds*, 2018, 753: 740-747.
- B Li, W Zhang, W Zhang, et al. Preparation of Ni-W/SiC nanocomposite coatings by electrochemical deposition. *Journal of Alloys and Compounds*, 2017, 702: 38-50.
- Y Lv, Y Ding, H Cui, et al. Investigation of microscopic residual stress and its effects on stress corrosion behavior of NiAl bronze alloy using in situ neutron diffraction/EBSD/tensile corrosion experiment. *Materials Characterization*, 2020, 164: 110351.
- F Zhang, R Ji, Y Liu, et al. Defect-rich engineering and F dopant co-modulated NiO hollow dendritic skeleton as a self-supported electrode for high-current density hydrogen evolution reaction. *Chemical Engineering Journal*, 2020: 126037.
- F Zhang, R Ji, Y Liu, et al. A novel nickel-based honeycomb electrode with microtapered holes and abundant multivacancies for highly efficient overall water splitting. *Applied Catalysis B: Environmental*, 2020, 276: 119141.
- R Ji, F Zhang, Y Liu, et al. Simple synthesis of a vacancy-rich NiO 2D/3D dendritic self-supported electrode for efficient overall water splitting. *Nanoscale*, 2019, 11.
- Q Liu, X Cao, A Du, et al. Investigation on adhesion strength and corrosion resistance of Ti-Zr aminotrimethylene phosphonic acid composite conversion coating on 7A52 aluminum alloy. *Applied Surface Science*, 2018, 458: 350-359.
- H J M Soares, O S Campos, D F Dias, et al. Chemical, morphological and corrosion characterisations of electrodeposited Ni-Fe-P coatings. *Electrochimica Acta*, 2018, 284: 18-23.
- Z Chai, C Jiang. Corrosion behavior and product film formation of Ni-Co-Cu nanocrystalline coatings in neutral salt environments. *Electrochimica Acta*, 2019, 298: 616-629.
- Z Mei, S Bhattacharya, A M Yacout. Adhesion of ZrN and Al₂O₃ coatings on U metal from first-principles. *Applied Surface Science*, 2019, 473: 121-126.
- D Yin, X Peng, Y Qin, et al. Quantifying adhesion energy of mechanical coatings at atomistic scale. *Applied Surface Science*, 2011, 258(4): 1451-1455.